

# Condensation in the Cathode of a PEM Fuel Cell

M. J. Kermani<sup>\*†</sup> J. M. Stockie<sup>\*</sup> A. G. Gerber<sup>†</sup>

University of New Brunswick, Fredericton, NB, Canada, E3B 5A3

Email: M.Kermani@unb.ca, stockie@unb.ca, agerber@unb.ca.

## ABSTRACT

Three species condensing flow in the cathode of a Proton Exchange Membrane (PEM) fuel cell is studied numerically. The aim is to locate condensing regions in the electrode. This study has been done using a systematic, three-step approach: (1) an isothermal dry flow model; (2) a non-isothermal dry flow model; and (3) non-isothermal flow with phase-change. The isothermal model cannot provide reliable knowledge of the location of liquid water. However, moving to a non-isothermal, single-phase model can provide useful information about the location of wet regions that matches reasonably well with a multi-phase model, particularly when an equilibrium thermodynamic model is used in multi-phase model. However, to compute the amount of moisture generated a multi-phase model is needed.

## 1 INTRODUCTION

A fuel cell is an energy conversion system which has a very promising future. Not only do fuel cells convert the chemical energy of fuel directly into electricity, but they also operate continuously as long as fuel is supplied (rather than batteries which are simply energy storage devices). Fuel cells are an ideal replacement for internal combustion engines owing to their much higher efficiency from not being limited by the Carnot cycle [1], and they also have the potential to generate power with near-zero emissions. At present, both stationary and portable applications are being pursued for fuel cells [2].

The present work is part of an ongoing effort to carefully model individual elements of the PEM fuel cell, with a particular focus on mass, heat, and water transport in the porous electrodes. In this paper, our previous single-phase model for the cathode of a PEM fuel cell, [3], is extended, and the phenomenon of condensation is studied numerically. We consider a mixture consisting of three species,  $O_2$ ,  $H_2O$  and  $N_2$ , maintained at thermodynamic equilibrium, in which all species share a single temperature field. It is further assumed that the wet phase (liquid water) is homogeneously distributed within each control volume as a "fog." The individual velocity field of each species is different in general, and differs from the averaged velocity of the mixture.

<sup>\*</sup>Department of Mathematics and Statistics.

<sup>†</sup>Department of Mechanical Engineering.

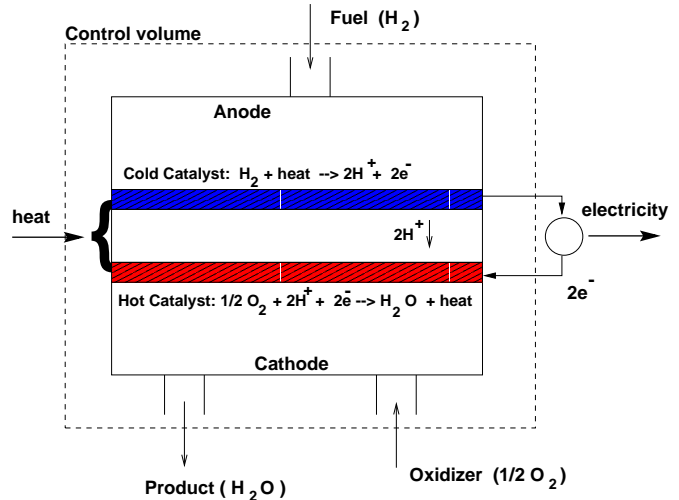
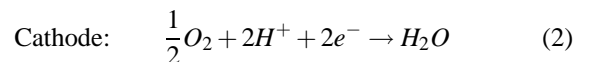
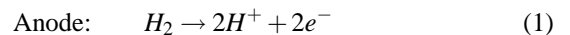


Figure 1: A schematic picture of a PEM fuel cell.

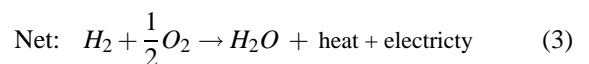
These diffusion velocities require the use of the Maxwell-Stefan equations in mixtures of three or more components. The scope of the undergoing project is described below.

### 1.1 Problem Definition

Figure 1 contains a schematic of a PEM fuel cell, which consists of two electrodes, the anode (hydrogen supply source) and the cathode (oxygen supply source), between which is sandwiched a polymer membrane usually consisting of Nafion<sup>®</sup>. The interfaces between the electrodes and membrane are impregnated with a platinum catalyst. The chemical reactions taking place at each electrode are given by:



The anode reaction absorbs heat while the process at the cathode is exothermic. The net reaction produces heat and electrical energy, and is determined by adding Eqns. 1 and 2:



Water is generated at the membrane-electrode interface, which humidifies the membrane thereby resulting in better proton conductivity in the membrane. However, excessive condensation can lead to blockage of the pores in the electrode, hence reducing the supply of oxygen and “choking” the cell. For these reasons there is great interest on understanding condensation phenomena in fuel cells, and in answering the following: *Question 1*: “Where does condensation occur?” and *Question 2*: “How much condensation appears?” The aim of the present paper is to answer these questions.

To better understand condensation phenomena in the fuel cell cathode, the present study is performed in three stages, moving from (1) an isothermal dry flow computation, to (2) a non-isothermal dry flow model, and finally to (3) non-isothermal flow with phase change. The first model cannot provide a reliable knowledge of the location of liquid water. Question 1 can be answered using the non-isothermal dry flow model, but unfortunately no conclusion can be drawn about the quantity of condensate. Therefore, Question 2 can only be dealt with reliably using the third, multi-phase model. The computation of non-isothermal multi-phase flow (Stage 3), which answers both Questions 1 and 2, is the main contribution of this paper.

## 2 MATHEMATICAL MODELLING

### 2.1 Governing Equations

The equations governing a wet-mixture consisting of three species,  $(1, 2, 3) = (\text{O}_2, \text{H}_2\text{O}, \text{N}_2)$ , are given below. In the absence of velocity slip between the steam components (liquid water and water vapor), the conservation equations of mass and energy for wet-mixture take an identical form of their dry-mixture counterparts [3]. Thus, for a general case of unsteady flow, the governing PDE's of a three-species mixture can be written as:

$$\frac{\partial}{\partial t}(\rho) = -\nabla \cdot (\rho \vec{V}), \quad (4)$$

$$\frac{\partial}{\partial t}(C_1) = -\nabla \cdot [C_1 \vec{V} + \vec{J}_1], \quad (5)$$

$$\frac{\partial}{\partial t}(C_2) = -\nabla \cdot [C_2 \vec{V} + \vec{J}_2], \quad (6)$$

$$\frac{\partial}{\partial t}(\rho e) = -\nabla \cdot (\rho \vec{V} h) + \nabla \cdot \vec{q} + \frac{i^2}{\sigma}. \quad (7)$$

Here,  $\rho$  is the mixture density which includes liquid water as well,  $\vec{V}$  is the mass-averaged velocity,  $C_1$  is the molar concentration of species 1 (oxygen),  $C_2$  is the molar concentration of species 2 (total water, i.e. water vapor + liquid water),  $\vec{J}_1$  and  $\vec{J}_2$  are molar diffusive fluxes based on mass-averaged velocity,  $e$  and  $h$  are the mixture internal energy and enthalpy,  $i$  is the current density, and  $\sigma$  is the electrical conductivity. The flux term,  $\vec{q}$ , consists of two parts: (i) a conductive heat flux, and (ii) a diffusive enthalpy flux arising

from the diffusion velocity, which takes into account the difference between the average velocity of mixture and species velocity. As a result,

$$\vec{q} = -\underbrace{\kappa \nabla T}_{(i)} + \underbrace{\sum_{i=1}^3 \bar{h}_i \vec{J}_i}_{(ii)}, \quad (8)$$

where  $\bar{h}_i$  is the molar specific enthalpy of species  $i$ ,  $T$  is the mixture temperature, and  $\kappa$  is the effective thermal conductivity. Numerical experiments for the dry case have shown that the size of term (ii) is several orders of magnitude smaller than (i) [4], and therefore we assume that  $\vec{q} \approx -\kappa \nabla T$  is a reasonable approximation for moist cases as well.

The mass averaged velocity of the mixture,  $\vec{V}$ , is related to the mixture pressure,  $P$ , via Darcy's law for flow in porous media,

$$\vec{V} = -\frac{K}{\epsilon \mu} \nabla P, \quad (9)$$

where  $\mu$  is the mixture viscosity,  $K$  is permeability and  $\epsilon$  is porosity. When condensation occurs in an electrode, it may lead to blockage of pores that inhibits the passage of reactant gases through the porous medium. This acts to reduce the effective porosity of the electrode, simulated by  $\epsilon = (1 - \beta) \epsilon_0$ , where  $\beta$  is the volume fraction of liquid water, and  $\epsilon_0$  is the porosity of the dry electrode.

Auxiliary equations are needed to obtain the diffusive fluxes  $\vec{J}_1$  and  $\vec{J}_2$ . In the simplest case, these fluxes are determined from Fick's law, which is only strictly valid for two-species mixtures [5], while the correct model for mixtures consisting of three species or more is the Maxwell-Stefan equations [5]. For complete information on how these fluxes are incorporated in Eqns. 5 and 6 and discretization of the PDE's 4–7, the reader is referred to [3]. The governing PDE's 4–7 are discretized in space using a central difference algorithm, and in time using an explicit forward Euler scheme.

### 2.2 Solution Procedure

Time integration of the governing PDE's 4–7 provides the conservative vector :

$$Q \equiv [q_1, q_2, q_3, q_4]^T = [\rho, C_1, C_2, \rho e]^T, \quad (10)$$

at each time step for any inner nodes. At each time step, the solution represents a fixed thermodynamic state point, which is then used to obtain moisture contents in the mixture. This solution procedure is explained through the following steps and in Sections 2.3 and 2.4.

1. Internal energy and concentration of the mixture:

$$e = q_4 / \rho, \quad (11)$$

$$C = C_1 + C_2 + (\rho - \rho_1 - \rho_2) / M_3, \quad (12)$$

where  $\rho_1 = C_1 M_1$  and  $\rho_2 = C_2 M_2$  are the density of oxygen and moist steam, respectively, and  $M_1$  and  $M_2$  are the molecular weight of oxygen and water.

2. Mole fraction of Species 1–3:

$$y_1 = C_1/C, \quad y_2 = C_2/C, \quad y_3 = 1 - y_1 - y_2. \quad (13)$$

3. Molecular weight, specific heat at constant volume, and molar internal energy of the mixture:

$$M = y_1 M_1 + y_2 M_2 + y_3 M_3, \quad (14)$$

$$\bar{C}_v = y_1 \bar{C}_{v1} + y_2 \bar{C}_{v2} + y_3 \bar{C}_{v3}, \quad (15)$$

$$\bar{e} = M e, \quad (16)$$

where  $M_3$  is the molecular weight of nitrogen,  $\bar{C}_{v1}$ ,  $\bar{C}_{v2}$ , and  $\bar{C}_{v3}$  are the specific heat at constant volume for oxygen, water vapor, and nitrogen, respectively.

At this stage in the computation, one can determine whether the flow is dry or wet. This decision is made based upon lagged values of temperature  $T$  and saturation temperature  $T_{sat}$ , in which  $T_{sat}$  is obtained using the local partial pressure of water,  $P_2$ . The flow is taken to be dry if  $T > T_{sat}$ , and is otherwise assumed to be wet. Both  $T$  and  $T_{sat}$  are updated at the end of each time step.

### 2.3 Dry Flow Computation ( $T > T_{sat}$ )

The final equations required to close the system for the dry case are as follows. The mixture temperature is obtained from mixture internal energy and specific heat via  $T = \bar{e}/\bar{C}_v$ . The entire dry flow is assumed to obey the ideal gas law, so that mixture pressure is determined using  $P = CR_0T$ , where  $R_0 = 8.31451 \times 10^7$  dyne/(mole · K) is the universal gas constant. The partial pressure of water vapor in dry case is  $P_2 = y_2 P$ . The saturation temperature,  $T_{sat}$ , is updated using the local value of  $P_2$  and a polynomial curve fit to the steam data which relates  $T$  and  $P_{sat}$ , as detailed in Appendix A.

### 2.4 Wet Flow Computation ( $T \leq T_{sat}$ )

In the case of wet flow, the state point is determined based on steam internal energy and density. The steam density is already known to be  $\rho_2 = C_2 M_2$ . The steam internal energy is determined by subtracting those portions of the internal energy belonging to oxygen and nitrogen from that of the mixture. However, at this stage the temperature of the mixture is unknown, which suggests the use of an iterative procedure to obtain mixture temperature.

From the wide range of iterative methods, the Newton–Raphson algorithm was found to converge very fast; however, it sometimes captures a physically-incorrect root. So instead, we have chosen to use a “binary search” algorithm,

which although slower in convergence, is very robust and always identifies the physically-correct root, if any root exists within the specified temperature interval.

The initial interval,  $T_{min} \leq T \leq T_{max}$ , is chosen large enough to cover a wide range of operating temperatures, e.g.  $T_{min} = 300$  K and  $T_{max} = 400$  K. The binary search algorithm is described as follows:

1. Calculate the “mid” temperature:

$$T_{mid} = (T_{min} + T_{max})/2. \quad (17)$$

2. Determine the internal energy of steam (total water):

$$e_2 = (\bar{e} - y_1 \bar{C}_{v1} T_{mid} - y_3 \bar{C}_{v3} T_{mid}) / (y_2 M_2). \quad (18)$$

3. Find the “quality,” the mass fraction of water vapor to that of steam:

$$\chi = (e_2 - e_f) / e_{fg}, \quad (19)$$

where  $e_f$  is the internal energy of saturated liquid, and  $e_{fg}$  is the internal energy of evaporation, which are functions only of the saturation temperature as indicated in Appendix A.

4. Obtain density of water vapor (it is assumed that the vapor portion of water obeys ideal gas law):

$$\rho_{2g} = \frac{M_2 P_{sat}(T_{mid})}{R_0 T_{mid}}, \quad (20)$$

5. Calculate steam density at  $T_{mid}$ :

$$\rho_{2_{T_{mid}}} = \rho_{2g} / \chi. \quad (21)$$

If  $\rho_2 > \rho_{2_{T_{mid}}}$  we take  $T_{min} = T_{mid}$ , otherwise  $T_{max} = T_{min}$ .

Steps 1–5 above are repeated until  $|\rho_2 - \rho_{2_{T_{mid}}}|$  becomes small enough. At this point,  $T = T_{mid}$ ,  $P_2 = P_{sat}(T_{mid})$ , and mixture pressure is the sum of the partial pressures:

$$P = (C_1 + C_3)R_0T + P_2, \quad (22)$$

where  $C_1 + C_3 = C - C_2$ .

For either the dry or wet case, mixture enthalpy is obtained from:

$$h = e + P/\rho. \quad (23)$$

### 2.5 Boundary Conditions

Throughout the following discussion of boundary conditions, refer to Fig. 2. At boundary locations (I), the wall is assumed to be impermeable. That is,  $J_1^y = J_2^y = 0$ , and  $v = 0$ ,

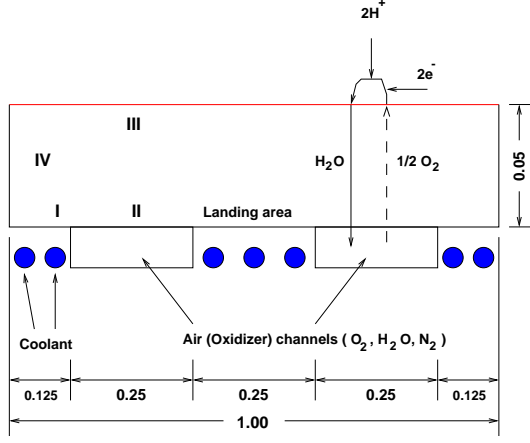


Figure 2: The cathode (computational domain) under consideration in the present study (all dimensions in *cm*).

where  $J_k^y$  and  $v$  represent diffusive flux and velocity components in vertical direction. The heat flux conducted through this boundary is given by  $-\kappa(\partial T/\partial y) = K_T^W(T^W - T)$ , where  $K_T^W$  is an equivalent convective heat transfer coefficient between the electrode and coolant, and  $T^W$  is the coolant temperature.

At the open channel boundary (II), the mixture pressure is set equal to the channel pressure,  $P = \bar{P}$ . The diffusive fluxes at this boundary are assumed to obey an analogue of Newton's law of cooling in heat transfer, i.e.  $J_k^y = r_0^k(\bar{C}_k - C_k)$ , for  $k = 1, 2$ , where  $r_0^k$  is the convective mass transfer coefficient for species  $k$ . The energy equation at this boundary is approximated by  $-\kappa(\partial T/\partial y) = K_T^C(\bar{T} - T)$ , where  $K_T^C$  is the convective heat transfer coefficient in the channel and  $\bar{T}$  is the channel temperature.

At the catalyst boundary (III), species 1 (oxygen) is assumed to obey the mass flux condition  $J_1^y = r_H(C_1 - C_\infty)$ , where  $r_H$  is the convective mass transfer coefficient and  $C_\infty$  is the concentration at the membrane, usually taken equal to zero. Water vapor (species 2) is generated at this boundary at the rate of two moles of water for each mole of oxygen that crosses the cathode-catalyst boundary; hence,  $N_2^y = -2N_1^y$ . The inert gas component, species 3 ( $N_2$ ), cannot penetrate the membrane which is impermeable to gas, and so  $N_3^y = 0$ . A heat flux arises at this boundary due to the heat of reaction, and hence  $\kappa(\partial T/\partial y) = 2N_1^y h_r$ , where  $h_r$  is the enthalpy of formation of water in gas form. At the side boundaries (IV), periodic boundary conditions are specified.

### 2.5.1 Moisture at boundaries

Moisture content at the boundaries cannot be determined directly using the boundary conditions prescribed in Section 2.5, and we describe next how  $\chi$  is calculated.

It can be shown that the boundary conditions at boundaries I, II and III determine boundary values of mixture pressure

( $P$ ), temperature ( $T$ ) and mole fraction of oxygen and water ( $y_1$  and  $y_2$ ). To obtain  $\chi$  at the boundary, we first need to determine whether the flow is dry or wet at the boundary. Flow at the boundary is dry if  $\phi < 1$ , where  $\phi = y_2 P / P_{sat}(T)$ , otherwise the boundary is wet. For a wet boundary, the quality can be computed from:

$$\chi = \frac{P_{sat}(T)}{C_2 R_0 T}, \quad (24)$$

where  $C_2 = y_2 C$  and  $C$  is determined from:

$$C = \frac{P - P_{sat}(T)}{(1 - y_2) R_0 T}. \quad (25)$$

## 3 RESULTS

A series of dry flow validations were carried out in an earlier publication [3], in which comparisons were made with those of [6, 7, 8, 9]. Also the wet flow algorithm of the condensing component, as described in Sections 2.2–2.4, has previously been validated vs. experimental data for a condensing pure steam [10]. In Sections 3.1–3.3 condensing regions are predicted in the cathode of a PEM fuel cell using (1) isothermal dry flow model; (2) non-isothermal dry flow model; and (3) non-isothermal flow with phase-change, and the results are discussed.

### 3.1 Isothermal Dry Flow

A schematic of the cathode being considered here is depicted in Fig. 2. A model for isothermal dry gas flow consisting of three species  $O_2$ ,  $H_2O$ , and  $N_2$  was developed for the cathode in [6], and over-saturated regions were located in [3]. The parameters used in this computation are as follows: permeability  $K = 10^{-8} \text{ cm}^2$ , porosity  $\epsilon_0 = 0.74$ , viscosity  $\mu = 2.24 \times 10^{-4} \text{ g/(cm s)}$ , binary diffusivity coefficients  $\Delta_{12} = 0.124$ ,  $\Delta_{13} = 0.104$  and  $\Delta_{23} = 0.123 \text{ cm}^2/\text{s}$ , channel pressure  $\bar{P} = 1.0 \times 10^6 \text{ dyne/cm}^2$ , species mole fractions in the channel  $y_1 = 0.21$ ,  $y_2 = 0.10$  and  $y_3 = 0.69$ , channel temperature  $\bar{T} = 346.15 \text{ }^\circ\text{K}$  ( $73 \text{ }^\circ\text{C}$ ), and mass transfer coefficients  $r_0^1 = r_0^2 = 10 \text{ cm/s}$  and  $r_H = 0.8 \text{ cm/s}$ .

Figure 3 shows the over-saturated regions obtained by an isothermal dry simulation. As shown in these unsteady simulations, the flow remains dry up to a certain time, after which over-saturated regions (the pockets colored in red) start to form at the top boundary and extend down to the bottom boundary. The condensing pockets shrink as the steady state condition is reached.

### 3.2 Non-Isothermal Dry Flow

In this section, we consider an extension to the isothermal model of Section 3.1, which adds the mixture's energy equation to the system of conservation equations. This non-

isothermal algorithm is the same as that developed in [3], with some new results showing the evolution of the over-saturated regions.

The problem parameters used in this non-isothermal case are:  $\kappa = 0.677 \times 10^5 \text{ erg}/(\text{cm s } ^\circ\text{K})$ ,  $\bar{C}_{v1}$ ,  $\bar{C}_{v2}$ ,  $\bar{C}_{v3}$  respectively  $= 2.14 \times 10^8$ ,  $2.55 \times 10^8$ , and  $2.08 \times 10^8 \text{ erg}/(\text{mol } ^\circ\text{K})$ ,  $K_T^C = 1.5 \times 10^5 \text{ erg}/(\text{s cm}^2 \text{ } ^\circ\text{K})$ ,  $K_T^W = 1.1 \times 10^7 \text{ erg}/(\text{s cm}^2 \text{ } ^\circ\text{K})$ ,  $T^W = 346.15^\circ\text{K}$ ,  $h_r = 2.418 \times 10^{12} \text{ erg/mol}$ ,  $i = 1.0 \text{ amp}/\text{cm}^2$ , and  $\sigma = 7.273 \times 10^{-5} \text{ amp}^2 \text{ s}/(\text{erg cm})$ . The rest of parameters are similar to the test case of Section 3.1.

Figure 4 shows predictions of over-saturated regions using non-isothermal dry simulations. As shown in this figure flow remains dry up to a certain time, after which condensation pockets (over-saturated regions) start to form at the bottom boundary above the landing area (the solid boundary lying between the channels and the edges of the computational domain, see Fig. 2). This is in stark contrast with the isothermal case in which condensation starts from the top boundary. However, the condensing pockets shrink (similar to the isothermal predictions) as the steady state is approached. Besides, the size of these pockets are much smaller than those in isothermal case. These significant differences in the location and size of the over-saturated regions between the isothermal study in the previous section and the non-isothermal simulations are explained as follows.

In the non-isothermal model there are two means disturbing the isothermal temperature field in the cathode (i) the heat source as indicated by  $i^2/\sigma$  in Eqn. 7, and (ii) the heat produced as the result of exothermic chemical reaction at the cathode-catalyst boundary. The size of over-saturated regions in non-isothermal case are smaller than those in isothermal case because of both of these means (i) and (ii), which enhance the temperature field and subsequently dry out the moisture. On the other hand, the shift in the location of over-saturated regions is only due to the exothermic cathodic reaction that takes place at the membrane/cathode boundary and rises the local temperature (the temperature of top boundary) and dries out the region.

### 3.3 Non-Isothermal Flow with Phase-Change

In the third stage of the present project, we extend the dry model of the previous section to allow for phase change. This is the main contribution of the present paper. To this end, an equilibrium thermodynamic model is used in which we assume that condensation begins as soon as the saturation line is crossed.

The problem parameters used in this case are those of Section 3.2. Figure 5 shows the time evolution of condensing regions predicted by the non-isothermal multi-phase model with  $\bar{T} = T^W = 73^\circ\text{C}$ , where  $\bar{T}$  and  $T^W$  are channel and coolant temperature, respectively. Over-saturated regions predicted in Section 3.2 match very well with the condens-

ing regions (see Figs. 4 and 5). However, the present step is needed to quantify the amount of moisture generated. The parameter quality,  $\chi$ , the mass fraction of water vapor to total water is used to quantify the amount of moisture produced.

Figures 6–8 show the results for a case of reduced channel and coolant temperature of  $\bar{T} = T^W = 65^\circ\text{C}$ , using the non-isothermal multi-phase model. Figure 6 (top) shows the condensing regions in this reduced temperature, predicting a much larger condensing regions when compared to those of Fig. 5. Figure 6 (middle) shows the contour plots for quality. As shown in this figure, about 50% of the mass of water is predicted to be in the form of liquid in the landing area. This is significant amount in terms of mass. Contours of relative humidity ( $\phi = P_2/P_{sat}$ ) is shown in Fig. 6 (bottom). At the wet regions (regions of  $\chi < 1$  in Fig. 6 (middle)), partial pressure of water vapor and the saturated pressure are equal. This gives  $\phi = 1$  in the wet regions.

Velocity vectors, configuration of streamlines, and contours of partial pressure for the oxygen and water species are shown in Figs. 7 and 8, respectively. As shown in these figures, oxygen is flowing toward the catalyst layer, and water generated at this layer returns back toward the channel. Also illustrious from these figures, the motion of oxygen and water are primarily determined based on their own partial pressure. That is, the higher value of partial pressure of oxygen at channel boundary drives oxygen toward the catalyst layer. On the other hand, water moves in opposite direction due to the revers direction in the gradient of partial pressure of water vapor.

## 4 CONCLUSION

The highlights of the present study are:

- A mathematical model has been given to model three-species isothermal, non-isothermal, dry or wet flow in the cathode of a PEM fuel cell.
- Isothermal computations give large sizes of over-saturated pockets starting from the catalyst boundary and extending toward the landing area.
- Non-isothermal dry model predicts tiny pockets of over-saturated regions when compared to isothermal case. This is due to temperature field enhancements caused by: (i) heat sources, uniformly distributed throughout the computational domain, and (ii) the exothermic chemical reaction at the catalyst boundary.
- Over-saturated regions predicted by the non-isothermal dry model well match with those of non-isothermal multi-phase model.
- Non-isothermal dry simulations cannot provide any information on the quantity of generated liquid water. To quantify the amount of liquid water, a non-isothermal multi-phase model is required.

- Significant amount of liquid water could be generated if the cell's operating temperature is reduced.

## Appendix A

The saturation pressure for steam is determined by a fifth order polynomial least square curve fit to the steam data taken from [11], given by:

$$p_{sat} = A_5\psi^5 + A_4\psi^4 + A_3\psi^3 + A_2\psi^2 + A_1\psi + A_0,$$

where  $\psi = T - t_0$ ,  $t_0 = 273.15$ , and  $p$  and  $T$  are in terms of dyne/cm<sup>2</sup> and K. The coefficients are

$$\begin{aligned} A_5 &= +1.777491E - 5, & A_4 &= +5.818105E - 3, \\ A_3 &= -8.508110E - 2, & A_2 &= +3.282638E + 1, \\ A_1 &= +1.313809E + 1, & A_0 &= +9.635916E + 3. \end{aligned}$$

Internal energy is obtained by a parabolic curve fit to the steam data taken from [11]:

$$e_{fg} = E_2\psi^2 + E_1\psi + E_0,$$

where  $e$  and  $T$  are in terms of erg/g and  $K$ ,

$$\begin{aligned} E_2 &= -0.00000196412464E + 6, \\ E_1 &= -0.00266166511681E + 6, \\ E_0 &= +2.37267810643234E + 6, \end{aligned}$$

and  $e_f = e_g - e_{fg}$ , where  $e_g = C_{v2}T$ .

## Acknowledgment

Financial support for this research was provided by grants from the Natural Sciences and Engineering Research Council of Canada (NSERC) and from Ballard Power Systems through the MITACS Network of Centres of Excellence.

## REFERENCES

- [1] Cengel, Y. A., and Boles, M. A., "Thermodynamics: An Engineering Approach," 4th ed., McGraw-Hill, 2001.
- [2] <http://www.ballard.com>.
- [3] Kermani, M. J., and Stockie, J. M., "Heat and Mass Transfer Modeling of Dry Gases in the Cathode of PEM Fuel Cells," *Int. J. Comput. Fluid Dyn.*, to appear, 2003.
- [4] Kermani, M. J., "Modified form of Energy Equation to Include Species Diffusive Fluxes," Unpublished report, Department of Mathematics and Statistics, University of New Brunswick, Fredericton, Canada, (Available upon request from M.Kermani@unb.ca), June 2002.
- [5] Taylor, R., and Krishna, R. "Multicomponent Mass Transfer," John Wiley and Sons, New York, 1993.

- [6] Stockie, J. M., Promislow, K. and Wetton, B. R., "A Finite Volume Method for Multicomponent Gas Transport in a Porous Fuel Cell Electrode," *Int. J. Numer. Meth. Fluids*, **41**:577–599, 2003.
- [7] Bradean, R. P., Promislow, K., and Wetton, B. R. "Heat and Mass Transfer in Porous Fuel Cell Electrodes" (2001) In *Proceedings of the International Symposium on Advances in Computational Heat Transfer*, Queensland, Australia, May 2001.
- [8] Um, S., Wang, C. Y. and Chen, K. S. (2000) "Computational Fluid Dynamics Modeling of Proton Exchange Membrane Fuel Cells", *J. Electrochem. Soc.* **147** 4485–4493.
- [9] Bernardi, D. M. and Verbrugge (1991) "Mathematical Model of a Gas Diffusion Electrode Bonded to a Polymer Electrolyte", *AIChE J.* **37** (8) 1151–1163.
- [10] Kermani, M. J., Gerber, A. G., and Stockie, J. M., "Thermodynamically Based Moisture Prediction Using Roe's Scheme," The 4th Conference of Iranian AeroSpace Society, Amir Kabir University of Technology, Tehran, Iran, January 27-29, 2003.
- [11] Moran, M. J., and Shapiro, H. N., "Fundamentals of Engineering Thermodynamics," 4th Ed., John Wiley & Sons, 1998.

Over-saturation regions; predictions by isothermal dry model

t = 0 to 0.11 Sec.



t = 0.115 Sec. (over-saturation onset)



t = 0.14 Sec.



t = 0.16 Sec.



t = 0.25 Sec. (maximum size of over-saturation pocket)



t = 0.6 Sec. (steady-state is achieved)



Figure 3: Time evolution of over-saturated regions (shaded in red) using the isothermal dry simulations ( $T = 73^{\circ}\text{C}$ ).

Over-saturation regions; predictions by non-isothermal dry model

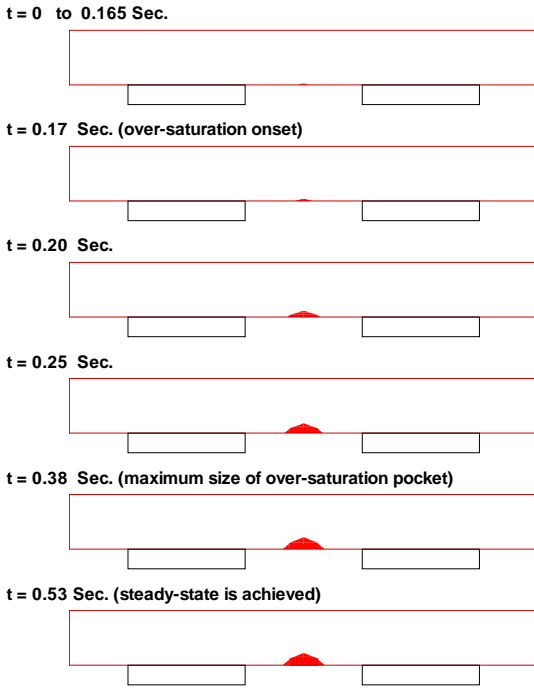


Figure 4: Time evolution of over-saturated regions (shaded in red) using non-isothermal dry simulations ( $\bar{T} = T^W = 73^\circ\text{C}$ , where  $\bar{T}$  and  $T^W$  are channel and coolant temp.)

Condensing regions; predictions by non-isothermal multi-phase model

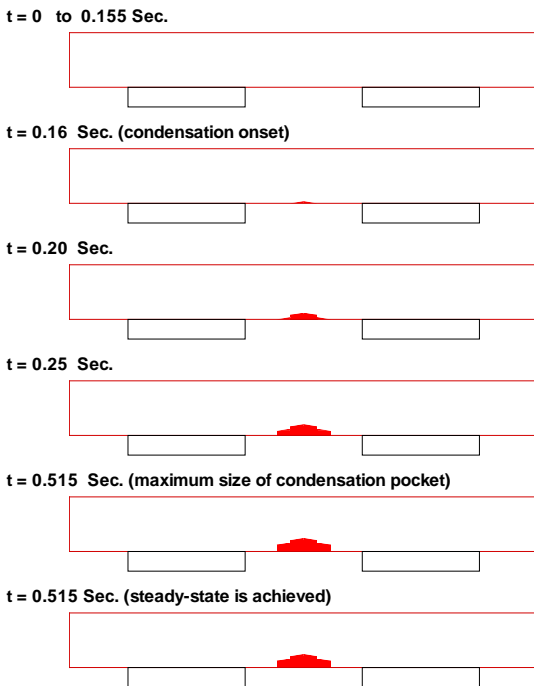


Figure 5: Time evolution of condensing regions (shaded in red) using non-isothermal multi-phase model ( $\bar{T} = T^W = 73^\circ\text{C}$ , where  $\bar{T}$  and  $T^W$  are channel and coolant temperature, respectively).

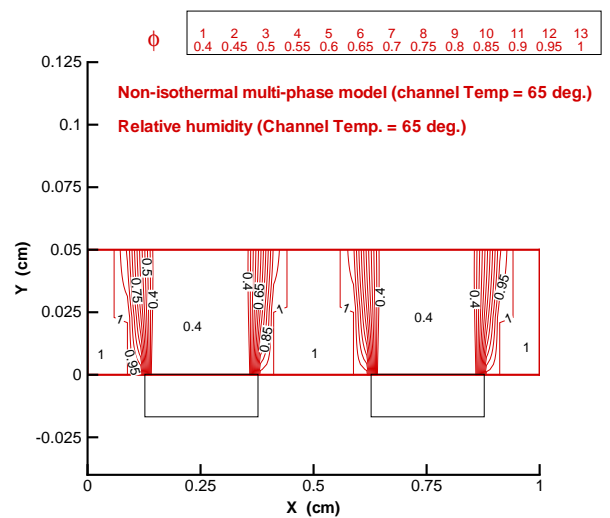
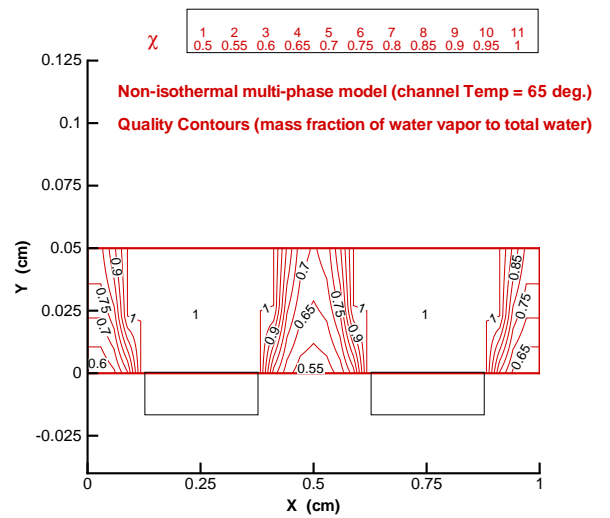
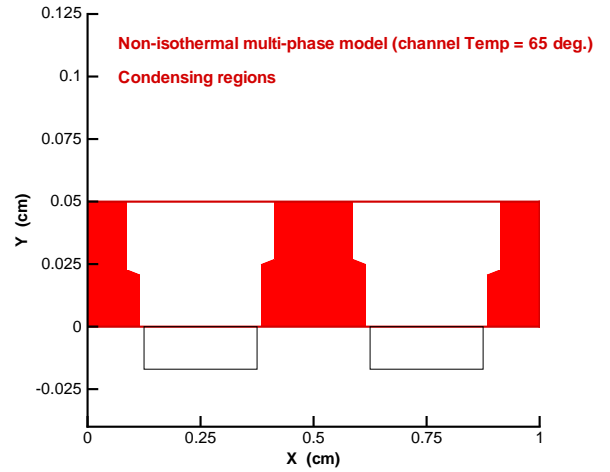


Figure 6: Results obtained using non-isothermal multi-phase model at channel and coolant temperature of  $65^\circ\text{C}$ . (Top) Condensing regions (shaded in red), (Middle) Quality contours (mass fraction of water vapor to that of total water), (Bottom) Relative humidity.

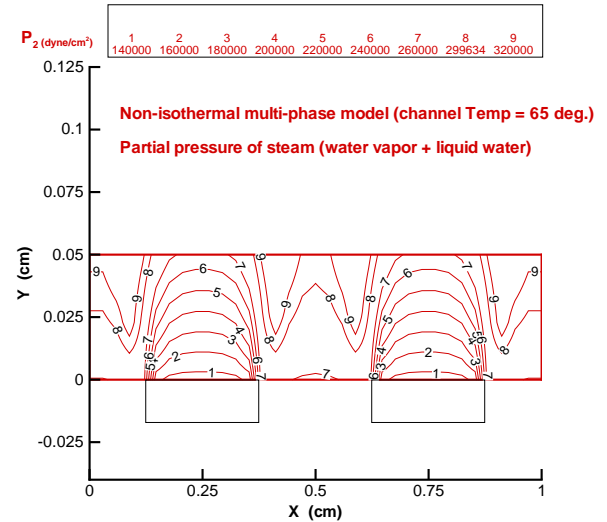
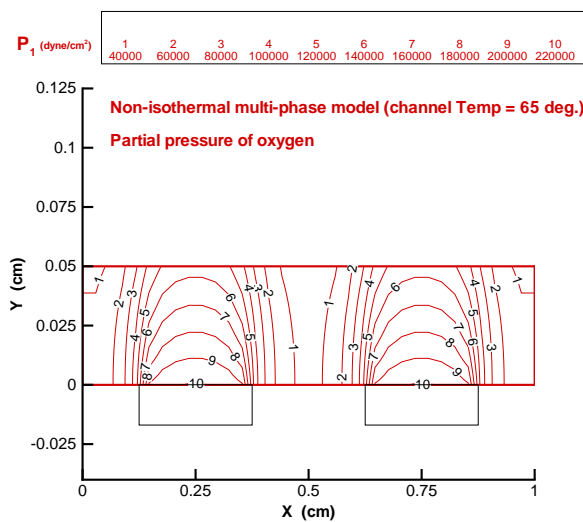
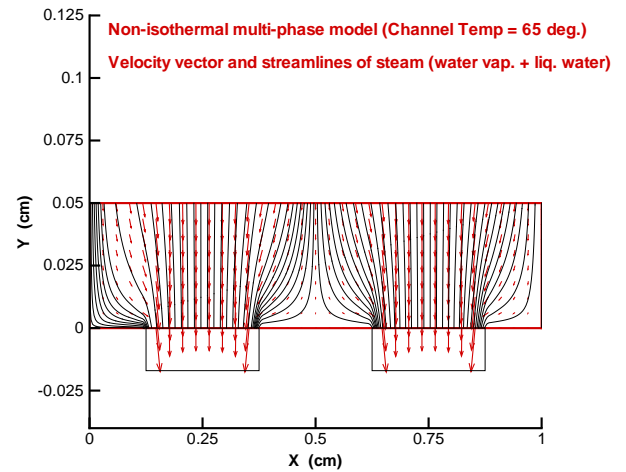
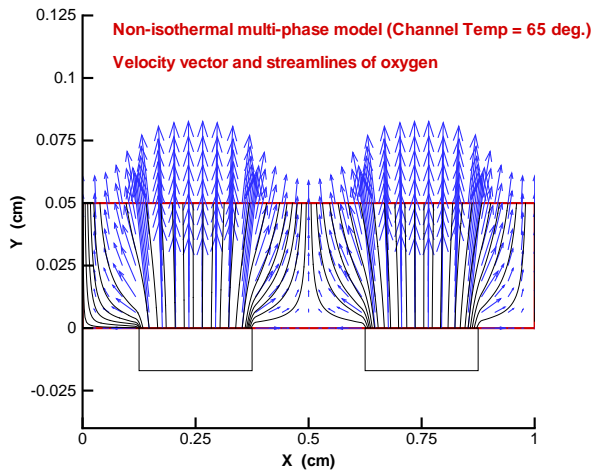


Figure 7: Results obtained using non-isothermal multi-phase model at channel and coolant temperature of 65 °C. (Top) Velocity vectors and streamlines of oxygen showing oxygen component flowing toward the catalyst layer. (Bottom) Partial pressure of oxygen. Shown in these figures oxygen is driven primarily by its own partial pressure, (i.e. higher value of partial pressure of oxygen at channel boundary drives oxygen toward the catalyst layer).

Figure 8: Results obtained using non-isothermal multi-phase model at channel and coolant temperature of 65 °C. (Top) Velocity vectors and streamlines of steam (water vapor + liquid water) showing steam (water) component flowing toward the channel. (Bottom) Partial pressure of water. Shown in these figures water is driven primarily by its own partial pressure, (i.e. higher value of partial pressure of water at the catalyst boundary drives water toward the channels).